JOURNAL OF SOLID STATE CHEMISTRY 86, 149–159 (1990)

Nonstoichiometry in $BaFeO_{3-y}$ ($0.35 < y < 0.50$)

J. M. GONZALEZ-CALBET, M. PARRAS, AND M. VALLET-REGI

Depto. Química Inorganica, Facultad de Ciencias Químicas, Universidad Complutense, 28040-Madrid, Spain

AND J. C. GRENIER

Laboratoire de Chimie du Solide du CNRS, Université de Bordeaux I, 33405 Talence-Cedex, France

Received October 11, 1989; in revised form February 12, 1990

$BaFeO_{3-y}$ compositions ($0.35 < y < 0.50$) annealed in the temperature range 980 to 1050°C have been investigated by means of electron diffraction and microscopy to resolve contradictory results from previous X-ray diffraction data. For $0.46 < y < 0.50$, the nonstoichiometry is accommodated through the formation of microdomains. Each of these domains shows a superstructure of the cubic perovskite structure with either a monoclinic symmetry (as observed in $Ba_2Fe_2O_5$) or an orthorhombic symmetry which is typical of a phase of composition $0.44 < y \leq 0.46$. With increase in the amount of Fe^{4+} ($0.35 < y \leq 0.44$), $BaFeO_{3-y}$ consists of a two-phase mixture of a 6H hexagonal phase and of the above orthorhombic phase. The limit of pure cubic stacking seems to be $y \simeq 0.46$.

Introduction

The $BaFeO_{3-y}$ system has been studied extensively (*1–10*) in order to identify the different phases $BaFe^{3+}_{1-\tau}Fe^{4+}_{\tau}O_{3-y}$ as a function of the anionic deficiency (y). In most cases, these phases were described using only powder X-ray diffraction data (XRD), and contradictory results were obtained.

In order to study how the nonstoichiometry is accommodated when the composition varies, we have reinvestigated this system by means of electron diffraction (ED) and microscopy (TEM). Two different hexagonal structural types exist for y values lower than 0.35 (*11*). For $0.07 \leq y < 0.13$, a 12H-hexagonal type appears (*12*) isostructural of $BaCrO_3$ (*13*) while for $0.20 \leq y \leq 0.25$, a single 6H-type structure is observed (*14*), isostructural with $BaTiO_3$ (*15*). For $0.25 \leq y \leq 0.35$, a phase of average composition $BaFeO_{2.75}$ intergrows, in a disordered way, with a cubic phase of composition close to $BaFeO_{2.50}$ (*14*).

On the other hand, an ED study of $Ba_2Fe_2O_5$, i.e., $y = 0.50$ (*16*), has revealed this phase to have a monoclinic symmetry with unit-cell parameters which are a multiple of those of a cubic perovskite subcell whose values (*17*), refined using the profile analysis method (*18*), are $a = 6.969(1)$ Å; $b = 11.724(1)$ Å; $c = 23.431(5)$ Å; $\beta = 98.74(1)°$.

We describe in this paper a study, using ED and TEM, of the $BaFeO_{3-y}$ system in the composition range $0.35 < y < 0.50$.

0022-4596/90 $3.00

Experimental

$BaFeO_{3-y}$ samples ($0.35 < y < 0.50$) were prepared from decomposition of a solution of barium and iron nitrates, at 890°C. A material of $BaFeO_{2.56}$ composition was obtained as described in Ref. (*19*). Annealing for 48 hr at various temperatures led to the compounds listed in Table I.

Total iron and barium in the samples were determined using chemical analysis and gravimetric method, respectively.

In order to know the stoichiometry of each sample, the amount of Fe^{4+} was determined by titration with a $K_2Cr_2O_7$ solution after the samples were dissolved in 3 *N* HCl with an excess of Mohr's salt.

Powder X-ray diffraction patterns were performed on a SIEMENS-D500 diffractometer using Cu$K\alpha$ radiation.

Electron diffraction and microscopy were carried out on a JEOL 200CX electron microscope equipped with a ±30° goniometer stage, kindly lent to us by the INPG, Grenoble (France).

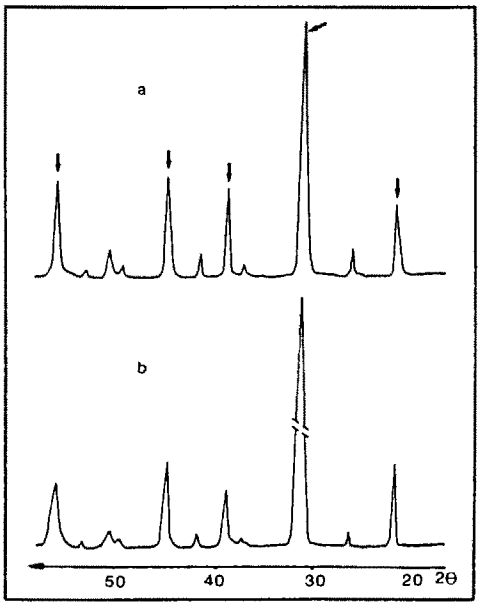

FIG. 1. Powder XRD patterns corresponding to $BaFeO_{2.64}$ (a) and $BaFeO_{2.60}$ (b) materials. Reflections corresponding to the pseudocubic perovskite subcell are marked with an arrow.

Results and Discussion

The average composition of the samples is shown in Table I: it can be seen that the amount of Fe^{4+} decreases as the annealing temperature increases. As previously mentioned (*14*), materials in the composition range $BaFeO_{2.80}$–$BaFeO_{2.65}$ have the 6H perovskite structural type (*15*), all their powder X-ray diffraction (XRD) patterns being similar to that of $BaTiO_3$. When the amount of Fe^{4+} decreases, some differences appear in the XRD data. Thus, Figs. 1a and 1b show the diffraction patterns corresponding to $BaFeO_{2.64}$ and $BaFeO_{2.60}$, respectively. First, a broadening of the diffraction maxima is observed with respect to the 6H phase. On the other hand, an increase in the relative intensity of the reflections corresponding to the pseudocubic perovskite subcell (marked with an arrow) is observed. Such differences can be more clearly appreciated in Fig. 2. Thus, Figs. 2a and 2c show, respectively, the diffraction patterns corresponding to a 6H hexagonal

TABLE I

MATERIALS SYNTHESIZED IN THE $BaFeO_{3-y}$ SYSTEM ($0.35 < y < 0.50$)

T (°C)	Fe^{4+} (%)[a]	Chemical composition
780	28	$BaFeO_{2.64}$
800	26	$BaFeO_{2.63}$
850	20	$BaFeO_{2.60}$
880	16	$BaFeO_{2.57}$
900	12	$BaFeO_{2.56}$
950	8	$BaFeO_{2.54}$
1000	4	$BaFeO_{2.52}$
1050	2δ[b]	$BaFeO_{2.50+\delta}$

[a] at% of total iron.
[b] $\delta \leq 0.01$.

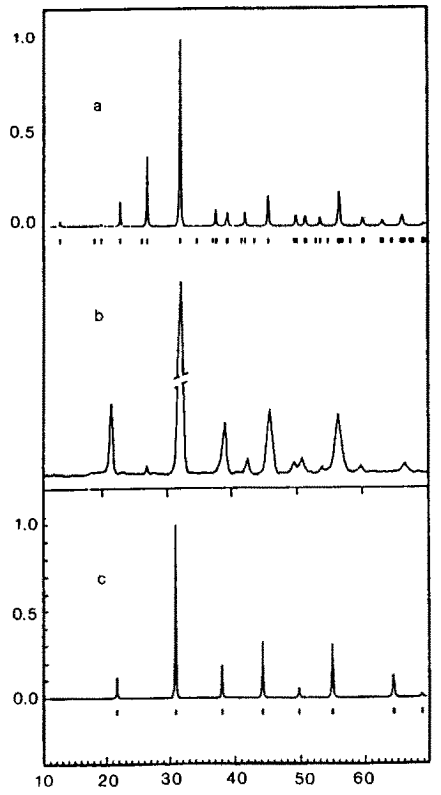

FIG. 2. (a) Powder XRD pattern of 6H $BaFeO_{2.75}$ calculated using the profile analysis method. (b) Experimental XRD pattern of $BaFeO_{2.60}$. (c) Powder XRD pattern of a hypothetical cubic perovskite "$BaFeO_3$" calculated using the Rietveld method.

phase with $BaFeO_{2.75}$ composition (unit-cell parameters: $a = 5.689(6)$, $c = 13.96(1)$ Å) and to a hypothetical cubic perovskite "$BaFeO_3$," with $a = 4$ Å, calculated using the Rietveld method. Figure 2b shows the experimental pattern of $BaFeO_{2.60}$ which appears close to that of the cubic phase.

In this way, the XRD patterns of both $BaFeO_{2.64}$ and $BaFeO_{2.60}$ can be interpreted as due to either the existence of a new hexagonal type with an increasing number of AO_3 layers with a cubic stacking compared to the 6H type (see the description of these structural types by Katz and Ward (*20*)), or to a phase mixture between a 6H hexagonal phase and a cubic phase. A study by electron diffraction, which we will discuss further on, is necessary to clarify this point.

In the powder XRD pattern of $BaFeO_{2.57}$ (Fig. 3a), it can be seen that only very few lines with low relative intensity, characteristic of a hexagonal phase, remain. Broad reflections could be indexed on the basis of a cubic perovskite phase with a unit-cell parameter $a \simeq 4.09$ Å.

The pattern of $BaFeO_{2.56}$ (Fig. 3b) exhibits a splitting of the intense 110_c peak and weak additional reflections can be observed. This pattern could be indexed with a tetragonal symmetry as previously reported by M. Zanne (*10*) ($a_t \simeq 2a_c$, $c_t \simeq 2a_c$, a_c being the cubic perovskite subcell parameter).

The XRD pattern of the $BaFeO_{2.54}$ sample is almost similar to the previous one,

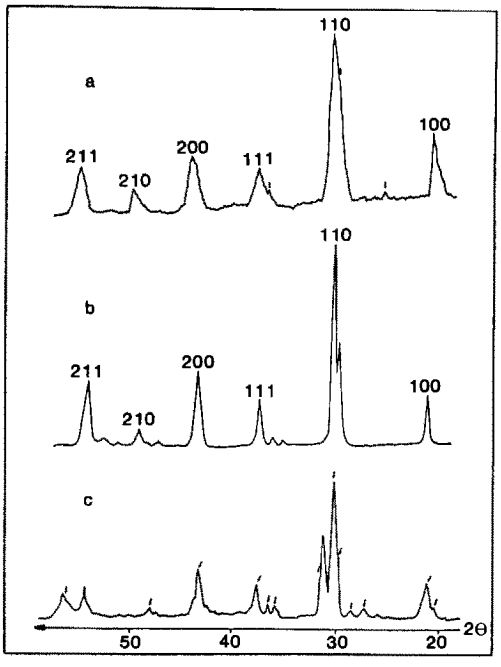

FIG. 3. XRD patterns corresponding to (a) $BaFeO_{2.57}$, (b) $BaFeO_{2.56}$, and (c) $BaFeO_{2.50+\delta}$.

the splitting of the line 110_c being more notable.

The pattern of the $BaFeO_{2.52}$ sample is close to that observed in $BaFeO_{2.54}$ but reflections corresponding to monoclinic $BaFeO_{2.50}$ can be already detected. This is emphasized in the $BaFeO_{2.50+\delta}$ XRD pattern (Fig. 3c) which appears very close to that of monoclinic $BaFeO_{2.50}$ (indicated by arrows in the figure). The peaks are, nevertheless, broadened.

Due to the broadening of the diffraction peaks in the $BaFeO_{2.60}$–$BaFeO_{2.50+\delta}$ samples, XRD data do not allow unambiguous determination of symmetry. However, since the reflections corresponding to the hexagonal close packing have progressively disappeared it seems that in this composition range the close packing is basically cubic.

Further study of the accommodation of the nonstoichiometry has been elucidated using electron diffraction and microscopy.

$BaFeO_{2.50+\delta}$–$BaFeO_{2.54}$

Figure 4a shows the ED pattern corresponding to the $BaFeO_{2.52}$ material along the $[1\bar{1}\bar{1}]_c$ zone axis; several sets of diffraction maxima can be observed. The corresponding electron micrograph is given in Fig. 4b. Several domains corresponding to the monoclinic $BaFeO_{2.50}$ material (d_{001} = 23.4 Å) (*16*) which intergrow with domains of a phase whose interplanar distance is around 10 Å are seen.

In a previous study (*21*), we have reported that monoclinic $BaFeO_{2.50}$ is beam sensitive and suffers a nonreversible phase transition during observation under the electron beam. The cell parameters of monoclinic $BaFeO_{2.50}$ are a multiple of those of a perovskite cell ($a_c\sqrt{3}$, $2a_c\sqrt{2}$, $a_c\sqrt{34}$) showing a 14-fold superlattice along the $(211)_c^*$ direction of the cubic subcell (*16*). After transformation under the beam, the new phase seems to be an orthorhombic perovskite superlattice with unit cell parameters $a_c\sqrt{3}$, $a_c\sqrt{2}$, $a_c\sqrt{6}$. This phase exhibits a 6-fold superlattice along the $(211)_c^*$ and equivalent directions leading to a microdomain texture (*21*).

According to these observations and on the basis of the domain texture observed in Fig. 4b, the ED pattern of Fig. 4a can be interpreted as the superposition of three types of diffraction maxima:

(1) Very strong spots corresponding to a cubic perovskite type substructure along the $[1\bar{1}\bar{1}]_c$ zone axis.

(2) Another set of maxima which can be interpreted as a superposition of three domains of monoclinic $BaFeO_{2.50}$, as schematically represented in Fig. 5, along the $[100]_m$ zone axis (subindex m refer to the monoclinic cell), showing a 14-fold superlattice along $(211)_c^*$ and equivalent directions.

(3) A series of maxima corresponding to three domains of the previously mentioned orthorhombic phase, as schematically shown in Fig. 6, where a 6-fold superlattice along $(211)_c^*$ and equivalent directions is seen.

This microdomain texture formed by the simultaneous presence of domains of the monoclinic phase and of the orthorhombic phase, leads to XRD patterns with broadened lines as previously described. The presence of both phases seems to be detected in these spectra since the relative intensities of the peaks change with the composition; the pure monoclinic phase is only obtained for $BaFeO_{2.50}$ (*16*).

$BaFeO_{2.54}$

With increase in the amount of Fe^{4+}, the monoclinic phase disappears, as can be seen in the ED pattern along $[1\bar{1}\bar{1}]_c$ of $BaFeO_{2.54}$ (Fig. 7a). All the spots can be indexed according to the three domains of the orthorhombic phase. The corresponding electron micrograph (Fig. 7b) shows only

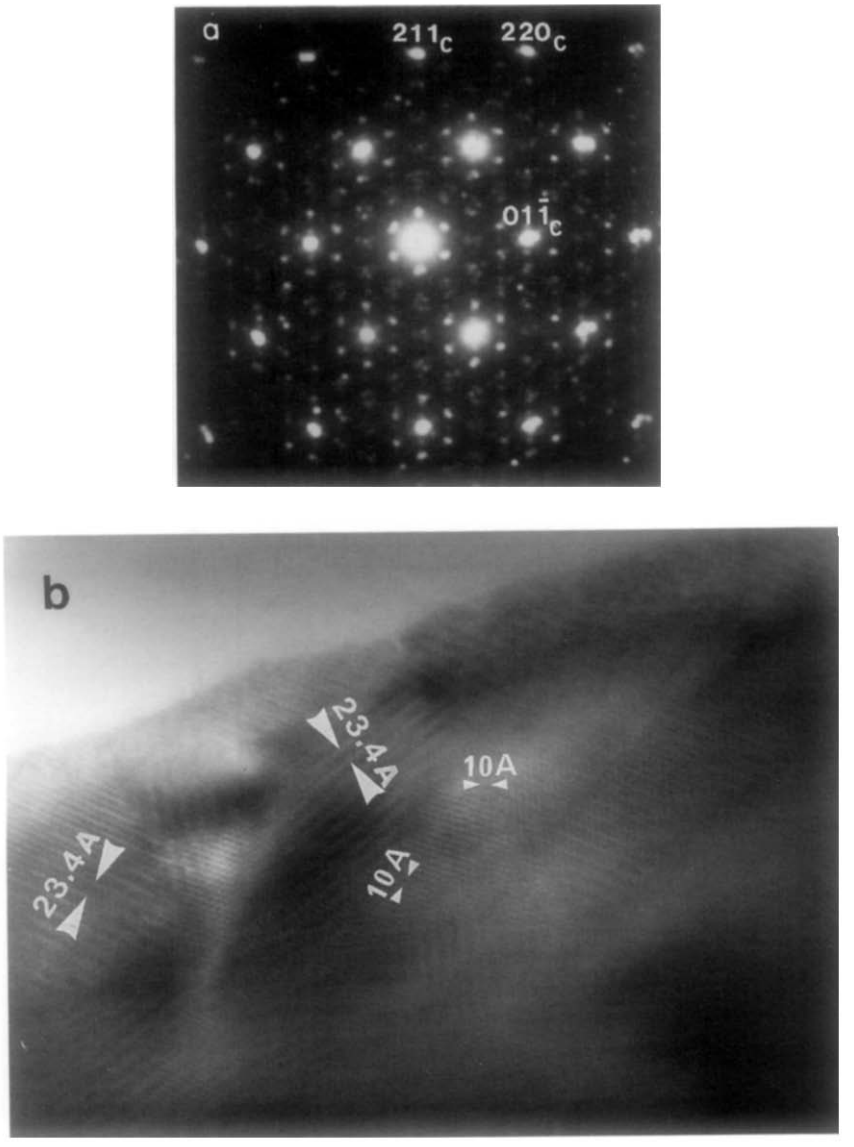

FIG. 4. (a) ED pattern of $BaFeO_{2.52}$ along the $[1\bar{1}\bar{1}]_c$ zone axis. (b) Corresponding electron micrograph.

the three domains of the orthorhombic phase at angles of 60° according to the observed fringes, which are along the $\bar{g}_{211c}$, $\bar{g}_{12\bar{1}c}$, and $\bar{g}_{1\bar{1}2c}$ directions.

By tilting around the $(211)_c^*$ axis, the electron diffraction pattern along the $[01\bar{1}]_c$ zone axis is obtained (Fig. 8a). No more than one domain is observed since in this projection, as schematically represented in Fig. 8b, only the 6-fold superlattice along the $(211)_c^*$ direction is seen.

In agreement with ED results, the XRD

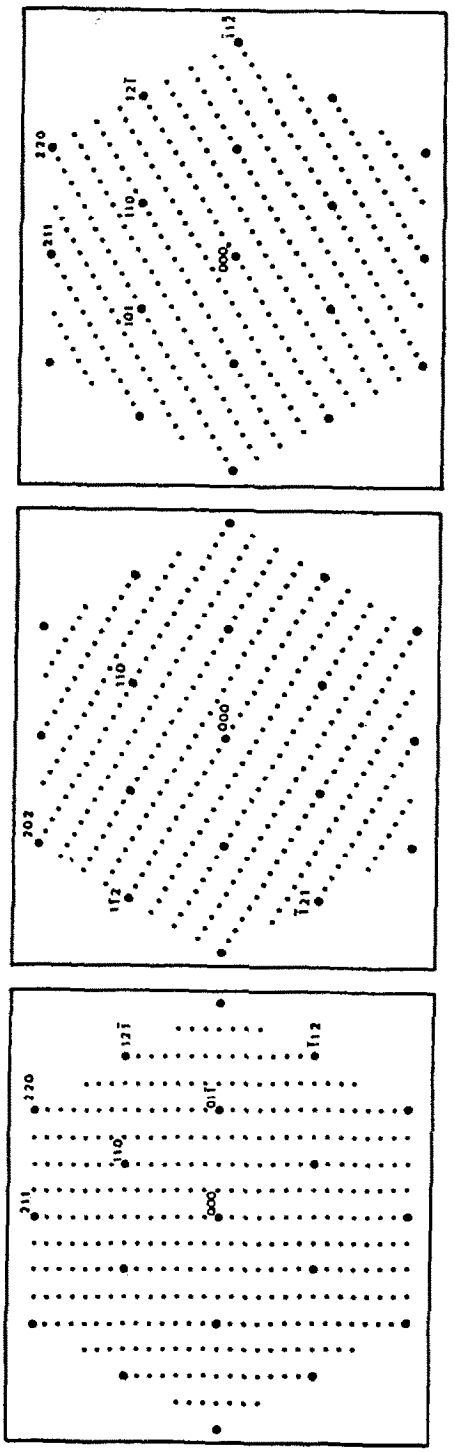

FIG. 5. Schematic representation of the ED patterns corresponding to the three domains of monoclinic $BaFeO_{2.50}$ following the (a) $\bar{g}_{211c}$, (b) $\bar{g}_{\bar{1}12c}$, and (c) $\bar{g}_{12\bar{1}c}$ directions.

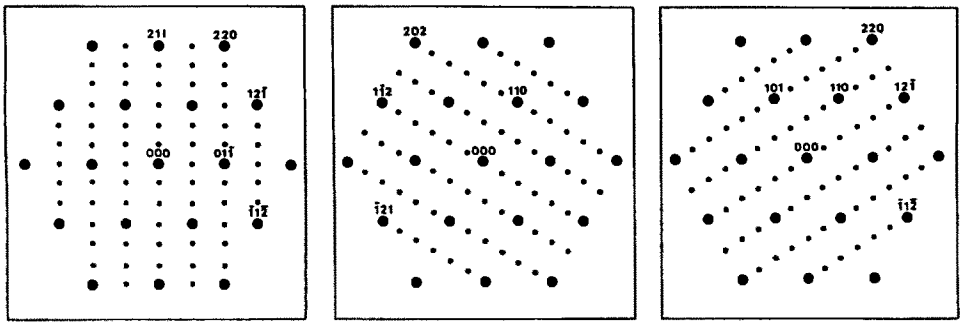

FIG. 6. Schematic representation of the ED patterns corresponding to the three domains of orthorhombic $BaFeO_{2.50}$ following the (a) $\vec{g}_{211c}$, (b) $\vec{g}_{1\bar{1}2c}$, and (c) $\vec{g}_{12\bar{1}c}$ directions.

pattern of $BaFeO_{2.54}$ is likely characteristic of a phase showing domains. Due to the observed domain texture, the diffraction peaks corresponding to the cubic sublattice are broadened and even split, and additional weak peaks appear. Indeed, this pattern can be indexed with the orthorhombic cell parameters determined by ED data ($a \simeq 7$ Å, $b \simeq 5.7$ Å, and $c \simeq 10$ Å) but refinement is not worthwhile as cell parameters are large and peaks little resolved as a consequence of the domain texture.

At this point it is worth mentioning that other perovskite-related ferrites (*22–26*) showing a domain texture also gave XRD patterns formed by relatively broad peaks indexable with a cubic perovskite-type unit cell, the real superstructure cell being determined only by electron diffraction. The formation of this phase is due to a random distribution of structural entities; due to the basic cube symmetry of the perovskite sublattice, this can happen in any of the three space directions.

When $BaFeO_{2.54}$ material is left for a few minutes under the electron beam a progressive decrease of the intensity of the superstructure spots is observed. Figure 9a shows the ED pattern along $[1\bar{1}\bar{1}]_c$ in the course of the transformation and Fig. 9b the same projection after complete transformation. Only the diffraction maxima corresponding to the cubic subcell remain. It is reasonable to think that the positions of heavy atoms such as barium and iron remain almost unchanged. After transformation under the electron beam, oxygen vacancies are likely distributed at random within the crystal and vacancy ordering of the orthorhombic phase has disappeared. Both phenomena obviously give cubic ED patterns.

In a previous study it has been shown that $Ca_2LaFe_3O_{8+z}$ reduces under the electron beam into two perovskite-related linephases, $Ca_2Fe_2O_5$ and $LaFeO_3$, which, under these conditions, appear to be thermodynamically more stable (*25*). In such a process, the elimination of oxygen is accompanied by the simultaneous diffusion of calcium and lanthanum ions, which according to available diffusion data are somewhat more mobile than Fe ions (*27, 28*). In $BaFeO_{2.54}$ only diffusion of oxygen ions must occur, as it is difficult to determine if a reduction process takes place since no ordered material is obtained.

$BaFeO_{2.56}$–$BaFeO_{2.64}$

Two types of crystals are observed in the $BaFeO_{2.56}$ material. The first one, which is by far the most abundant, shows ED pat-

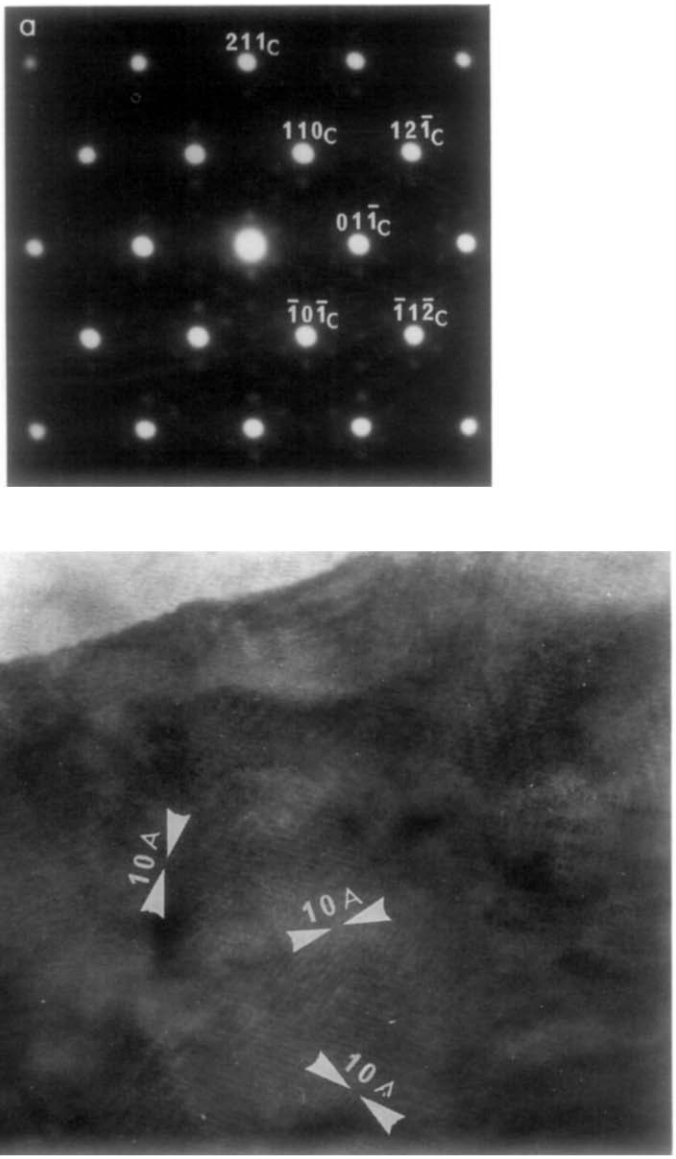

FIG. 7. (a) ED pattern of the $BaFeO_{2.54}$ material along the $[1\bar{1}\bar{1}]_c$ zone axis. Only weak superstructure spots of the orthorhombic phase are visible. (b) Corresponding electron micrograph showing three sets of domains in which interplanar distances of 10 Å are seen.

terns and micrographs similar to those previously described for the $BaFeO_{2.54}$. The second type are of the 6H structural type. The amount of this phase is so small that it cannot be observed by X-ray diffraction. It is worth recalling that this XRD pattern, indexed on the basis of a tetragonal phase by M. Zanne (*10*), corresponds in fact to the orthorhombic phase.

A similar situation is observed in

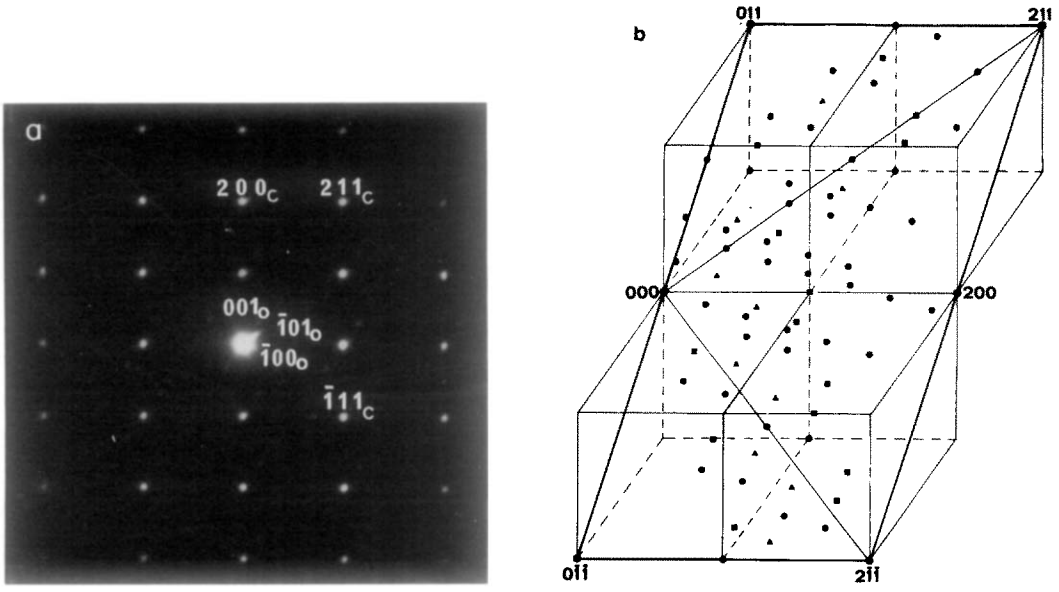

FIG. 8. (a) ED pattern of $BaFeO_{2.54}$ along the $[01\bar{1}]_c$ zone axis. Very weak superstructure spots are seen along the $(211)_c$ direction. (b) Schematic representation of the $(01\bar{1})_c$ reciprocal plane.

$BaFeO_{2.57}$, $BaFeO_{2.60}$, and $BaFeO_{2.64}$ samples; the amount of the 6H phase gradually increases with the Fe^{4+} content. As mentioned above, this is reflected in the corresponding XRD patterns characteristic of a two-phase composition range.

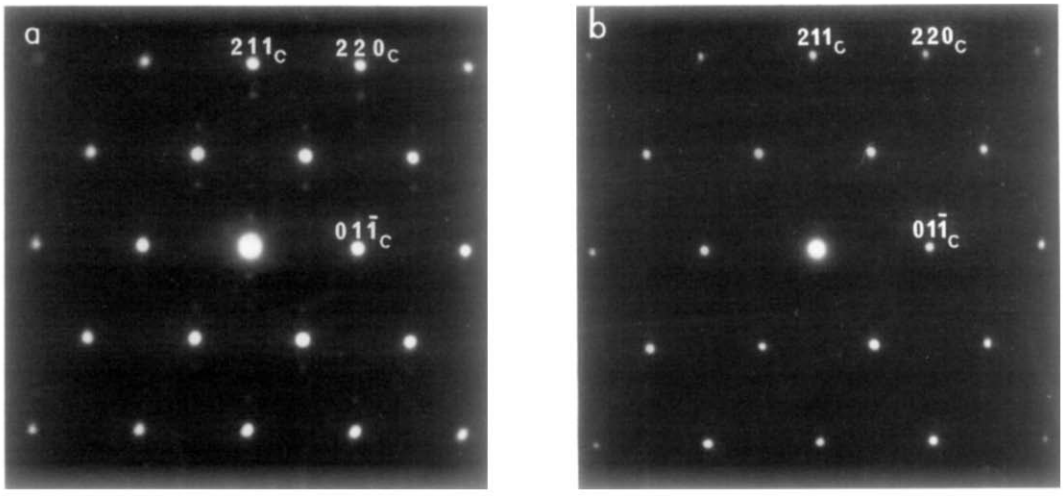

FIG. 9. ED pattern of $BaFeO_{2.54}$ along $[1\bar{1}\bar{1}]_c$ (a) at the beginning of the transformation under the electron beam and (b) after complete transformation.

Conclusion

According to these results, the $0.35 < y < 0.50$ composition range can be divided into three domains:

—$0.35 < y \leq 0.44$: $BaFeO_{2.65-2.56}$ — a two-phase mixture of the 6H hexagonal phase and of the orthorhombic phase with a microdomain texture.

—$0.44 < y \leq 0.46$: $BaFeO_{2.56-2.54}$ — a phase of orthorhombic symmetry in which the nonstoichiometry is accommodated through the formation of microdomains.

—$0.46 < y < 0.50$: $BaFeO_{2.54-2.50+\delta}$ — a phase showing the intergrowth of six types of domains: three corresponding to monoclinic $Ba_2Fe_2O_5$ and three to the previous orthorhombic phase.

The orthorhombic phase only exists in a very narrow composition range, 8 to 12% Fe^{4+} ($0.44 < y \leq 0.46$).

In a previous work (*19*), we have shown that the limit of composition of the pure hexagonal phase was $BaFeO_{2.65}$ (30% Fe^{4+}). We should note that for lower Fe^{4+} content, no other structural type intermediate between the 6H and 3C seems to appear. We think that either the orthorhombic phase or the monoclinic phase have cubic close packing, but vacancy ordering in these phases is obviously different and still unknown.

References

1. J. Frankuchen, R. Ward, and H. Erchark, *J. Amer. Chem. Soc.* **68,** 2805 (1946).
2. W. Malinofsky and H. Kedesdey, *J. Amer. Chem. Soc.* **76,** 3090 (1954).
3. S. W. Debyshire, A. C. Fraker, and H. Staldelmaier, *Acta Crystallogr.* **14,** 1293 (1961).
4. H. J. Van Hook, *J. Phys. Chem.* **68,** 3786 (1965).
5. J. B. MacChesney, J. F. Potter, R. C. Sherwood, and H. J. Williams, *J. Chem. Phys.* **43,** 3317 (1965).
6. S. Mori, *J. Amer. Ceram. Soc.* **49,** 600 (1966).
7. S. Mori, *J. Phys. Soc. Japan* **28,** 44 (1970).
8. T. Negas and R. Roth, *J. Res. Natl. Bur. Stand. Sect. A* **73**(4), 425 (1969).
9. B. E. Gushe, J. Frankuchen, and R. Ward, *J. Amer. Chem. Soc.* **79,** 5601 (1971).
10. M. Zanne, PhD thesis, University of Nancy (1973).
11. M. Vallet-Regi, M. Parras, J. M. Gonzalez-Calbet, and J. C. Grenier, "Advances in Ferrites, Proceedings of the Fifth International Conference on Ferrites, Bombay, India," p. 1143 (1989).
12. M. Parras, M. Vallet-Regi, J. M. Gonzalez-Calbet, J. C. Grenier, P. Hagenmuller, and J. R. Carvajal, *J. Eur. Inorg. Chem.* **26,** 299 (1989).
13. B. L. Chamberland, *Inorg. Chem.* **8,** 286 (1968).
14. M. Parras, M. Vallet-Regi, J. M. Gonzalez-Calbet, and J. C. Grenier, *J. Solid State Chem.* **85,** 121 (1989).
15. R. D. Burbank and H. T. Evans, *Acta Crystallogr.* **1,** 330 (1948).
16. M. Parras, M. Vallet-Regi, J. M. Gonzalez-Calbet, M. A. Alario-Franco, J. C. Grenier, and P. Hagenmuller, *Mater. Res. Bull.* **22,** 1413 (1987).
17. M. Parras, PhD thesis, University of Madrid (1988).
18. H. M. Rietveld, *Acta Crystallogr.* **22,** 151 (1967).
19. J. C. Grenier, A. Wattiaux, M. Pouchard, P. Hagenmuller, M. Parras, M. Vallet, J. M. Gonzalez-Calbet, and M. Alario, *J. Solid State Chem.* **80,** 6 (1989).
20. L. Katz and R. Ward, *Inorg. Chem.* **3**(2), 205 (1964).
21. J. M. Gonzalez-Calbet, M. Parras, M. Vallet-Regi, and J. C. Grenier, *J. Solid State Chem.*, in press.
22. M. Alario-Franco, M. J. R. Henche, M. Vallet-Regi, J. M. Gonzalez-Calbet, J. C. Grenier, A. Wattiaux, and P. Hagenmuller, *J. Solid State Chem.* **46,** 23 (1983).
23. M. A. Alario-Franco, J. M. Gonzalez-Calbet, M. Vallet-Regi, and J. C. Grenier, *J. Solid State Chem.* **49,** 219 (1983).
24. M. Vallet-Regi, J. M. Gonzalez-Calbet, J.

VERDE, AND M. A. ALARIO-FRANCO, *J. Solid State Chem.* **57,** 197 (1985).

25. J. M. GONZALEZ-CALBET, M. VALLET-REGI, AND M. A. ALARIO-FRANCO, *J. Solid State Chem.* **60,** 320 (1985).
26. J. M. GONZALEZ-CALBET, M. VALLET-REGI, J. ALONSO, J. R. CARVAJAL, AND J. FONTCUBERTA, *J. Solid State Chem.* **81,** 1 (1989).
27. I. E. SHIMANOVICH, M. M. PAULYUCHENKO, B. O. FILONOV, AND S. A. PROKUDINA, *Vesti Akad. Navuk BSSR, Ser. Khim. Navak* **6,** 61 (1969).
28. T. ISHIGAKI, S. YAMAUCHI, J. MIZUSAKI, K. FUEKI, H. NAITO, AND T. ADACHI, *J. Solid State Chem.* **55,** 50 (1984).
29. V. H. GOLDSCHIMIDT "Geochemische Verteilungs Gosetze der Elements VII–VIII" (1927–1928).
30. R. D. SHANNON AND C. T. PREWITT, *Acta Crystallogr. B* **25,** 925 (1969).